Int. J. Heat Mass Transfer. Vol. 32, No. 6, pp. 1141–1153, 1989
Printed in Great Britain

0017–9310/89 $3.00+0.00

Turbofan forced mixer/nozzle temperature and flow field modelling

P. KOUTMOS and J. J. McGUIRK
Fluids Section, Department of Mechanical Engineering, Imperial College, London SW7 2BX, U.K.

(*Received* 22 *September* 1988 *and in final form* 25 *November* 1988)

Abstract—A computational procedure is described for the calculation of the flow and temperature fields in a multilobed turbofan mixer/nozzle combination. The predictions have been obtained using a finite-volume solution procedure for the steady three-dimensional elliptic equations of fluid flow. The procedure allows the calculation of flows within complex geometries using a non-aligned mesh system so that the flow within the lobes themselves may be predicted. Turbulence is modelled using the two-equation k–ε eddy viscosity model. Forced mixer performance is shown to be dominated by a periodic array of axial vorticity cells created by the lobe geometry. The calculation of the large secondary velocities associated with this vorticity within and at exit from the lobes provided the necessary boundary conditions at the lobe exit for the predictions of the flow in the mixing duct region. This removes the dependency of previous calculation methods for mixing ducts on measured secondary velocities at the lobe exit plane. The present work demonstrates the capability of the current method to predict the downstream development of the large-scale secondary motions and their strong influence on the temperature signature at the nozzle exit. Results are also presented to illustrate the ability of the method to predict parameters of importance to mixer designers such as mixer total pressure loss and mixer efficiency. The plausibility of the results obtained illustrates the potential of the method to provide a flexible analysis technique for the complete mixer/nozzle system.

INTRODUCTION

IN CURRENT and future turbofan engines the use of forced mixers to help mix the hot core and cold bypass streams prior to exhaust through the exit nozzle is likely to be of increasing importance due to the potential improvements they offer in specific fuel consumption, thrust augmentation and jet noise reduction. If the internal cross stream heat transfer in these devices is arranged such that a more uniform total energy profile can be obtained at exit, a small but significant improvement in performance can result with a noticeable reduction in jet noise because of the decrease in maximum nozzle efflux velocities. The level of these gains depends on a balance between the efficiency of temperature mixing achieved and the extra pressure losses incurred in the mixing process. The most popular and successful mixer configuration in use is the lobed mixer (Fig. 1). This increases the interfacial area over which the two streams mix as well as the lateral scales within which the actual mixing takes place (from the incoming boundary layer thickness δ in undistorted annular mixers to the height of the lobe $h \gg \delta$, see Werle *et al.* [1]). Further, due to differing radial deflections, shear between the two streams is also increased and mixing promoted downstream of the lobes.

Due to the complexity of the lobe geometry (Fig. 1) the choice of the best configuration depends upon the selection of a large number of parameters. The lobe shape and degree of radial penetration, the plug and tailpipe angle and length, the use of scarfed or scalloped lobes (i.e. cut-outs in the lobe surfaces). Evidently, the traditional approach of identifying an optimum combination of this large number of parameters through model scale and then selective full scale testing is both expensive and time consuming. These difficulties have led to several studies into the adequacy and applicability of numerical procedures based on computational fluid dynamics techniques for predicting the flow field and heat transfer behaviour of forced mixers.

The majority of earlier efforts have concentrated on calculating the flow in the region between the exit plane of the lobes and the exit plane of the tailplane nozzle, i.e. the mixing duct itself. These computational studies have mainly involved three-dimensional parabolic versions of the governing equations which require only a single forward marching sweep through the mixing duct downstream of the lobe exit plane. Birch *et al.* [2] and Barton and Birch [3] have used the parabolic analysis of Patankar and Spalding [4], for flows with negligible streamwise diffusion. Kreskovsky *et al.* [5] and Povinelli and Anderson [6] have calculated mixing duct flows using an alternative method based on the primary/secondary velocity decomposition approach of Briley and McDonald [7]. This latter method is more general since it allows the inclusion of a pressure field determined from an *a priori* potential flow solution within the specified mixing duct geometry to introduce some elliptic effects into the streamwise momentum equations. These predictions have by and large been very encouraging

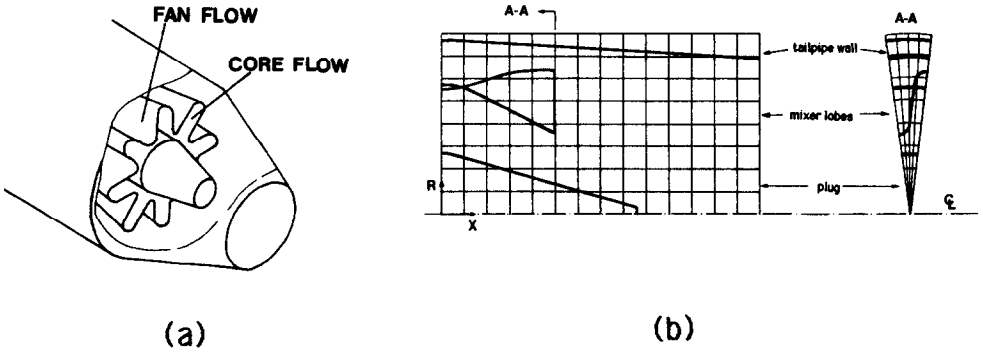

FIG. 1. (a) Sketch of typical lobed mixer geometry. (b) Side and end view showing mixer embedded within cylindrical polar grid.

when compared with the available measurements [6, 8]. Nevertheless all the published investigations have also emphasized that reasonable simulations of the flow and temperature patterns could only be obtained when the inlet three-dimensional velocity field at the lobe exit plane was known in sufficient detail. This is particularly important in view of the detailed experimental investigation of Paterson [9] which demonstrated the strong dominance of the complex lobe generated secondary flows on the nozzle mixing process. This fact, that the computational approaches adopted to date are dependent on the availability of suitable experimental data for inlet boundary conditions, clearly detracts from their usefulness as true prediction procedures.

An initial attempt to model the secondary flows within the lobe geometry itself and thus remove the above restriction has recently been reported by Barber *et al.* [10, 11]. They used inviscid concepts to predict the generation of the array of streamwise vortices at the lobe exit. A quasi-three-dimensional procedure was adopted based on a potential flow analysis and a zonal approach. A separation of variables technique was used and calculations were performed for a series of axisymmetric problems. The analysis was restricted to slender mixer lobes (the change in radius of which is small compared to their length) and is clearly only applicable if the flow remains attached to the lobe surface. Even then, the provision of truly representative initial conditions for the downstream mixing duct calculation would require the inviscid method to be interacted with a three-dimensional lobe boundary layer calculation. Certainly a potential flow model of the lobe flow is valuable in describing the gross features of the periodic distributions of circulation at the mixing plane but it is unlikely to be able to provide a detailed description of the exit velocities or the minor horseshoe like vortices which are believed to occur in some types of mixers (see ref. [8]). Further, no such detailed predictions of the flow structure have been reported with this method nor has its ability to calculate reliably the complete lobed mixer/nozzle system yet been demonstrated.

A different approach was adopted in ref. [12] which used a finite volume technique for the solution of the full three-dimensional elliptic equations of fluid flow, extended to allow the modelling of flows within complex geometries. Turbulence was modelled using the two-equation k–ε eddy viscosity model. In the basic method a simple cylindrical polar coordinate system was retained and the geometry of the lobe boundary was identified in the code via the specification of the intersections of the non-aligned mesh with the lobe surface. This enabled the determination of various types of boundary cells depending on their shape and position relative to the solid surface. This was followed by a formulation of appropriate modifications for the new finite-volume equations for each of these cells. The results of this investigation supported the capability of the method to predict the streamwise vorticity generated within the lobes.

In the above work attention was focused only on the lobe flow with the core and bypass streams being calculated separately. No attempt was made to calculate the heat transfer processes occurring within the mixing duct. Further, the compatibility which must be enforced as soon as the mixer wall separating the two streams ends and mixing begins was not satisfied. In reality, both streams must flow through the lobes towards the same pressure field at the mixer exit plane and this may have an upstream effect and alter the flow through the lobes. The present work aims to extend the work of ref. [12] and allow coupling between the lobe and mixing duct flows thus introducing the effects of the mixing in the tailpipe nozzle into the lobe flow development. This two-way coupling should provide a more realistic simulation of the secondary flows through the lobed mixer. The complete form of the governing equations and the three-dimensional arbitrary boundary method used for the lobe flow will also be used for the converging tailpipe nozzle flow. This increases the generality of the analysis since it allows steep gradients of the flow properties near the mixing plane and, if desired, significant radial and azimuthal variations in the tailpipe and plug geometry which might be encountered in reality. This

practice removes, for example, the difficulties experienced by the spatial marching codes in the vicinity of the plug end face. For example, the parabolic procedure of Povinelli and Anderson [6] required this region to be 'faired in' to exclude the zone where the parabolic assumptions would have failed. More significantly however the present mixing duct calculations will use inflow conditions provided solely by the lobe flow calculation; this means that prediction of the complete lobed mixer/tailpipe nozzle flow will be possible using only knowledge of the inlet boundary conditions at a plane just downstream of the outlet guide vanes—a position where they are much easier to prescribe than at the mixer exit.

MATHEMATICAL MODEL AND CALCULATION ARRANGEMENTS

The calculations presented here have been obtained by solving the full three-dimensional elliptic forms of the equations for conservation of mass, momentum and thermal energy in time-averaged form; using Cartesian tensor notation for convenience these may be written as

$$\frac{\partial}{\partial x_i}(\rho U_i) = 0$$

$$\frac{\partial}{\partial x_j}(\rho U_i U_j) = -\frac{\partial \bar{P}}{\partial x_i} - \frac{\partial}{\partial x_j}(\rho \overline{u_i u_j})$$

$$\frac{\partial}{\partial x_j}(\rho U_j T) = -\frac{\partial}{\partial x_j}(\rho \overline{u_j t})$$

where upper case letters represent time mean quantities and lower case letters fluctuating components. In the fan and core flow predictions the density has been assumed constant (although at different values in each stream) as the two streams were considered individually isothermal (at different temperatures) with relatively low Mach numbers and separated by an adiabatic wall. In the mixing duct calculations the flow was again assumed incompressible but the density was connected to the local temperature through the gas law $\rho = \bar{P}/RT$, where $\bar{P}$ is the mean pressure level in the mixing duct. This approach ignores the effect of temperature fluctuations on the mean gas density. For large temperature differences between hot core and bypass streams this simplification may be unacceptable. If necessary a pdf describing the scalar fluctuations may be introduced to allow a more correct treatment of the non-linear density/temperature relationship; this has not yet been included in the present model. The $\rho\overline{u_i u_j}$ and $\rho\overline{u_j t}$ in the above equations are the turbulent Reynolds stresses and heat fluxes, respectively. The former are here approximated via the high Reynolds number version of the two equation k–ε turbulence model introduced by Jones and Launder [13]. The Reynolds stress is linearly related to the mean rate of strain via a scalar turbulent viscosity

$$-\rho\overline{u_i u_j} = \mu_t\left[\frac{\partial U_i}{\partial x_j} + \frac{\partial U_j}{\partial x_i}\right] - \frac{2}{3}\delta_{ij}\rho k.$$

The turbulent heat flux is obtained using the turbulent Prandtl number approach

$$-\rho\overline{u_j t} = \frac{\mu_t}{\sigma_T}\frac{\partial T}{\partial x_j}.$$

In these expressions the turbulent viscosity is calculated from

$$\mu_t = C_\mu \rho \frac{k^2}{\varepsilon}$$

where k and ε are the turbulence kinetic energy and dissipation rate of turbulence energy, respectively, the values of which are obtained from solution of the modelled transport equations

$$\frac{\partial}{\partial x_j}(\rho U_j k) = \frac{\partial}{\partial x_j}\left(\frac{\mu_t}{\sigma_k}\frac{\partial k}{\partial x_j}\right) - \rho\overline{u_i u_j}\frac{\partial U_i}{\partial x_j} - \rho\varepsilon$$

$$\frac{\partial}{\partial x_j}(\rho U_j \varepsilon) = \frac{\partial}{\partial x_j}\left(\frac{\mu_t}{\sigma_\varepsilon}\frac{\partial \varepsilon}{\partial x_j}\right) - C_{\varepsilon 1}\frac{\varepsilon}{k}\rho\overline{u_i u_j}\frac{\partial U_i}{\partial x_j} - C_{\varepsilon 2}\rho\frac{\varepsilon^2}{k}.$$

The model contains five empirical constants which are assigned the following values, found to give good agreement in a wide range of two-dimensional shear flows [14]:

$$C_\mu = 0.09, \quad C_{\varepsilon 1} = 1.44, \quad C_{\varepsilon 2} = 1.92,$$

$$\sigma_k = 1.0, \quad \sigma_\varepsilon = 1.3, \quad \sigma_T = 0.9.$$

Such a simple turbulence model might be thought inappropriate, given the complexity of the present flow. However, the same model and an even simpler eddy viscosity model were used by Kreskovsky *et al.* [5] who found, at least for the mixing duct flow, that calculations of the secondary flow development were fairly insensitive to the turbulence model, apart from fine scale details. The generation of the streamwise vorticity is believed to be essentially an inviscid phenomena, so that the particular turbulence model used may not be too important, at least with respect to this part of the calculation. It is unlikely that improved turbulence models such as Reynolds stress transport will be required for this type of flow.

The solution of the above seven steady flow, three-dimensional coupled partial differential equations was obtained using a finite-volume scheme. The formulation comprised a linearized implicit conservative scheme using hybrid differencing for convective fluxes. The use of a higher order differencing scheme such as the QUICK algorithm would have helped to reduce possible false diffusion errors in the calculation of this complex three-dimensional flow. However, the implementation of the complex lobe geometry within the code was of primary importance in the current work; further development would be required to

allow a higher order scheme to be adopted within the framework of the complex lobe geometry treatment. Further, since the appearance of the strong cross-plane flows which characterize forced mixers are known to be strongly pressure dominated, it seemed worthwhile beginning the calculations with a lower order convection discretization before proceeding to more complicated and less numerically stable techniques. The method is formulated in terms of velocity and pressure using a staggered grid arrangement. The pressure velocity coupling is handled via the standard SIMPLE pressure correction algorithm [15]. The code has been used in several three-dimensional recirculating flow problems, including a study of primary zone flow patterns in a can type gas turbine combustor [16].

For the prediction of the flow within the three-dimensional geometry of the lobe and the tailpipe nozzle the method of ref. [12], as described in the Introduction, was adopted. Here only an outline of the method will be given, a more detailed description can be found in the above reference. In this procedure the numerical method described above remained unaltered including the use of a regular grid in a Cartesian or cylindrical polar solution domain. The arbitrary geometry of the lobes lies therefore within this regular non-aligned grid (see Fig. 1). The solid walls are represented in a piecewise planar approximation to the real surface; calculation of the intersection points between the surface and the staggered grids enables the identification of individual finite-volume cells which lie inside or outside the flow region. For cells which intersect with the boundary the intersection points are used to calculate the proportion of each of the six cell face areas which lie inside the flow region. The finite volume equations are then modified by taking these truncated or extended cell face areas into account.

The calculation of the complete mixer/tailpipe nozzle flow was divided into three stages. In the first stage the lobe flow prediction (domains A and B, Fig. 2) was obtained as described in ref. [12]. The inlet to these calculation domains is upstream of the lobes which are here assumed coplanar (i.e. perpendicular to the engine centre-line). The predicted fan and core flow exit momentum and temperature fields were then used as inlet boundary conditions for the calculation of the downstream domain C (Fig. 2). This calculation completes the first stage of the solution. The coupling between lobe flow and mixing duct flow is clearly incomplete, in the sense that it is as yet 'one way', i.e. the solution from domains A and B has influenced domain C, but not vice versa. The second stage introduces a two-way coupling between domains A–C. For this second stage calculation, the static pressure field at the inlet to the mixing duct predicted from the first stage is now used as the *downstream* boundary condition for the fan and core regions which are now re-calculated. This is a more realistic exit boundary condition for the two streams since it allows both flows to exit to the same pressure field. This also reflects the influence of the mixing taking place in the mixing duct onto the upstream developing flows. The use of this alternative downstream boundary condition allows the flow in the lobes to adjust itself to the mixing duct conditions during the second stage re-calculation of domains A and B. The modified lobe exit conditions are then used to re-calculate the mixing duct flow to complete the second stage. A third pass was also carried out to ensure that the iterative coupling procedure was sufficiently converged; the criterion for convergence was the relative changes in the pressure, velocity and temperature fields at the lobe and mixing duct exit planes obtained at each stage of the procedure. Intermediate and final results from this procedure will be presented in a following section.

MODELLED GEOMETRY AND BOUNDARY CONDITIONS

The 12 lobed mixer and the downstream mixing region considered in the present investigation are shown in Fig. 2. Flow symmetry and geometric periodic repeatability require a solution only for a sector formed by a 15° slice comprising half a lobe as shown in Fig. 2 and extending from a lobe peak to a lobe trough with symmetry boundary conditions along the edges of the sector. The same size sector was used for the representation of the downstream mixing duct with similar edge boundary conditions. A grid consisting of $40 \times 16 \times 22$ (R, θ, X) nodes (14000 mesh points) represented the cylindrical polar calculation domain for the lobe flow region. Particular attention was paid to the R–θ plane where the grid lines were uniformly spaced circumferentially every 1° for better resolution of the lobe contour. The same grid was used for both the fan and core flow predictions which were however performed independently of each other. This offers the advantage that only one set of intersections of the lobe surface with the grid is required for each calculation. A separate mesh consisting of $40 \times 16 \times 25$ (R, θ, X) grid nodes was used for the calculation of the mixing duct; in this region the R–θ grid node distribution was the same as for the fan and core regions to facilitate the transfer of data over the interface region in the coupling procedure between domains A–C. In the axial direction the mesh expanded with a ratio of 1.1. The first stage of the calculation was also performed with a coarser mesh of 9000 nodes (40% fewer than the above). The differences in the results between these two meshes were relatively minor (e.g. changes in the levels of the lobe exit secondary velocities by only about 5%) and suggest that the finer grid used for the calculation is acceptable. Finer grids would represent the modelled geometry more accurately but restrictions in available computer storage and time impose difficulties in the mesh refinement process. The mesh node density used here is in any case similar to that used by a number of other investigators [2, 6]. If further mesh node

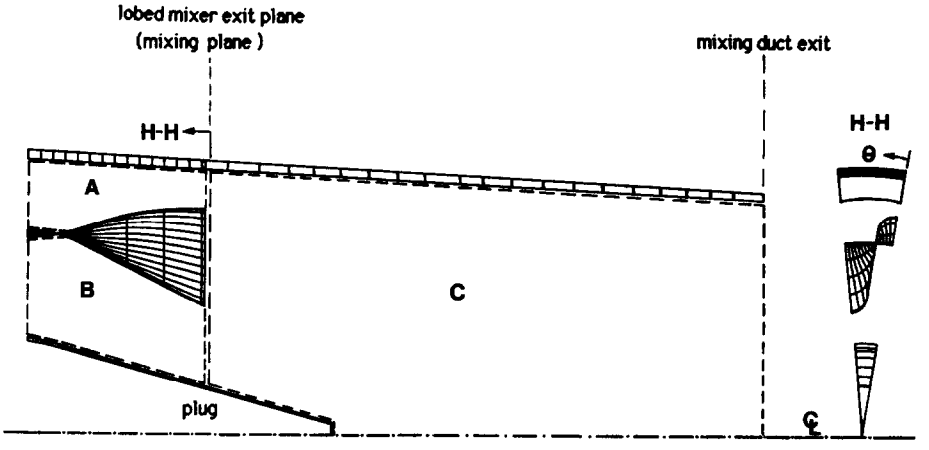

FIG. 2. Geometry of lobed mixer, downstream mixing duct and separate solution domains.

increases were to be made, it is the R–θ mesh which would be worthwhile of further refinement. In the axial direction the flow is predominantly along the mesh, at least in the mixing duct region where numerical diffusion effects in the scalar equation are likely to be largest.

The mass flows on the fan and core sides were 0.5 and 0.3 kg s^{-1}, with corresponding inlet air axial velocities of 125 and 143 m s^{-1}. At the upstream boundary, at the inlet of calculation domains A and B, the axial velocity profile was taken to be similar to that of fully developed annulus flow while the V and W components were assumed zero. Levels of turbulence kinetic energy were chosen as 3 and 5% for the fan and turbine streams, respectively. These values are similar to those used in a number of previous computational investigations of mixer flows [2, 6]. Inlet values for energy dissipation rate at this position were calculated using an assumption of a length scale proportional to the appropriate inlet annular height. The total temperature ratio between the fan and core streams was 0.67. As mentioned in the previous section the inlet values for the mixing duct calculation were the values of all dependent variables predicted at the exit plane from fan and core regions.

There are unfortunately no measurements available for the model lobed mixer which allow detailed comparisons with the predictions. Consequently results are first presented in terms of streakline plots to provide an overall qualitative assessment of the predicted flow patterns. This computational flow visualization is achieved by tracking weightless particles released from the grid nodes through the predicted velocity field (on a given two-dimensional plane) for a finite time (tracking time); this provides a quick and accurate method of illustrating the axial and azimuthal flow development along the length of the mixer. Temperature contours which depict the extent of thermal mixing between the two streams are also provided. The spatial positions at which the streakline and temperature contour plots were obtained are given in Table 1. In order to enable better visualization of the streakline plots the circumferential direction has been enlarged by a factor of 4 (the θ scale in these plots therefore goes from 0 to 60° rather than 0 to 15°). Similarly, the θ-direction in the temperature contour plots has been increased threefold. For R–θ planes streaklines have been obtained with a tracking time twice that used for the axial planes. Note also that the R–θ planes are shown from the viewpoint of someone looking downstream in the mixer.

RESULTS

Comparison of the differences in the predicted flow structure between the three stages of the coupling procedure as described earlier are shown first in Figs. 3–5. Figure 3 illustrates the cross-stream flow at plane i (located close to the mixing plane). These plots indicate that between the last two stages differences are very small and evidently confined to the vicinity of the lobe interface. Between the first and second stage calculations, the strength of the axial vorticity produced by the lobes has increased significantly but

Table 1

Axial ($X-R$) planes		
a	$\theta = 0°$	through lobe peak
b	$\theta = 7°$	midway between lobe peak and trough
c	$\theta = 15°$	through lobe trough
Azimuthal ($R-\theta$) planes		
d	$x/L_N = 0.015$	within lobes
e	$x/L_N = 0.084$	within lobes
f	$x/L_N = 0.146$	within lobes
g	$x/L_N = 0.215$	within lobes
h	$x/L_N = 0.300$	within lobes
i	$x/L_N = 0.305$	within mixing duct
j	$x/L_N = 0.43$	within mixing duct
k	$x/L_N = 1.0$	within mixing duct

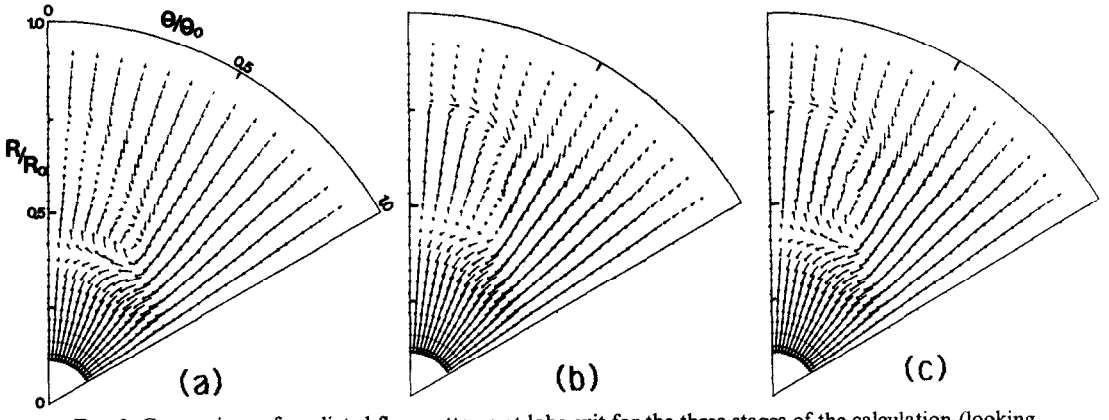

FIG. 3. Comparison of predicted flow patterns at lobe exit for the three stages of the calculation (looking downstream).

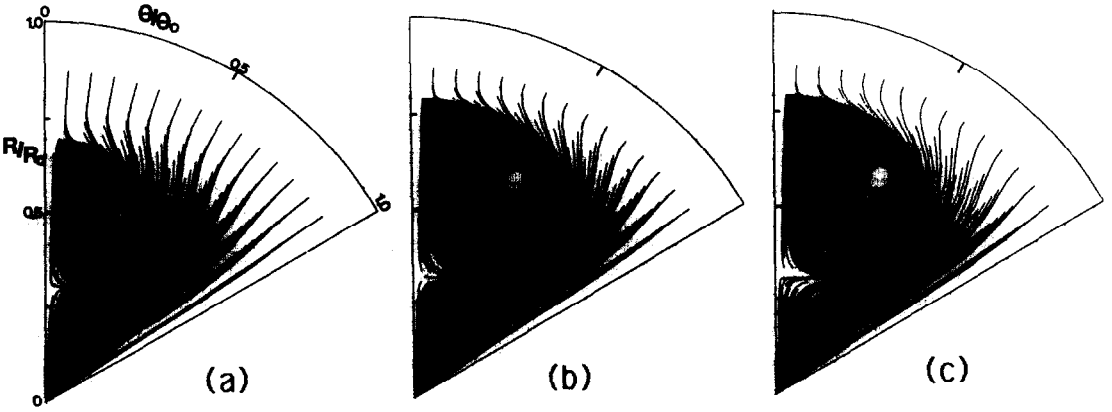

FIG. 4. Comparison of predicted flow patterns at mixing duct exit for the three stages of the calculation (looking downstream).

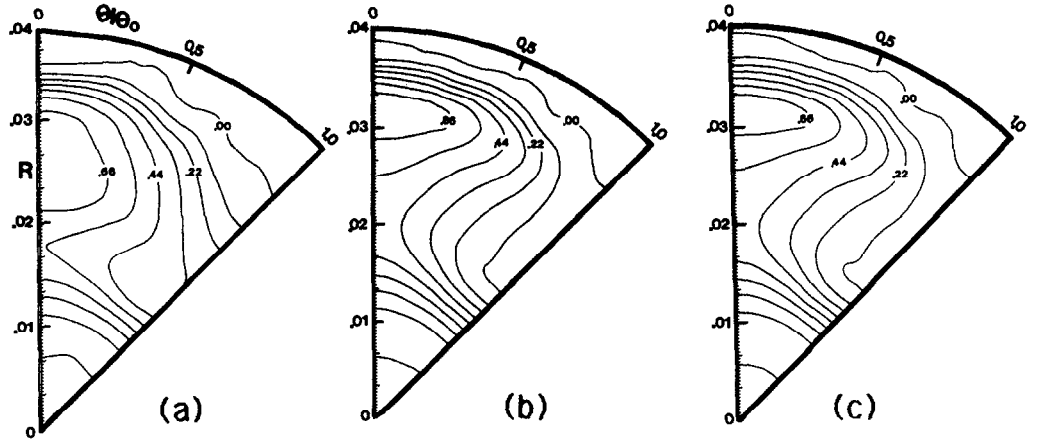

FIG. 5. Comparison of predicted normalized temperature (T^*) at mixing duct exit for the three stages of the calculation ($T^* = (T - T_{FAN})/(T_{CORE} - T_{FAN})$) (looking downstream).

remains about the same in the third stage with only small-scale changes. The outward radial flow in the lobe peak region (core side) has grown considerably when the mixing duct flow is taken into account. The secondary velocities decay slowly down the mixing duct, but are still present at the exit. This is illustrated in Fig. 4; the particle tracking time has been increased to ease visualization, each of the patterns again corresponds to a different stage in the coupling procedure. The differences are once more significant

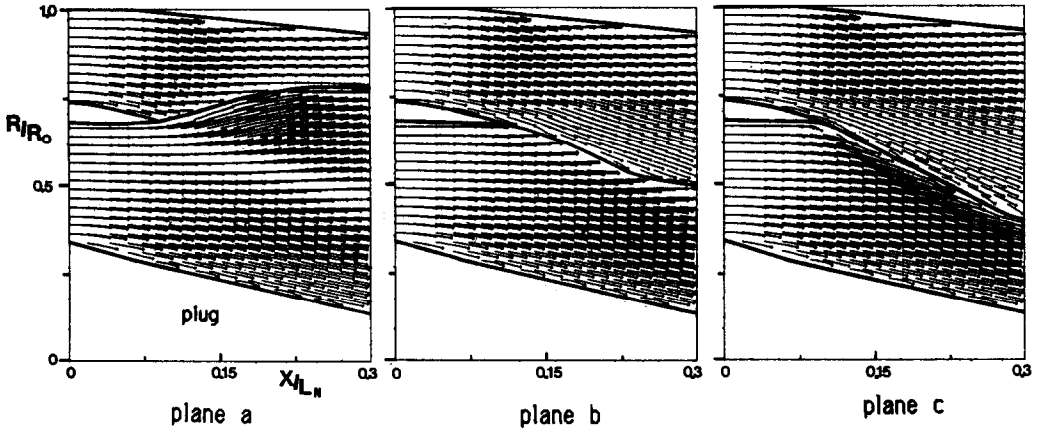

FIG. 6. Predicted flow patterns within lobed mixer: axial planes.

between the first two stages (Figs. 4(a) and (b)), both qualitatively (change in location and shape of predicted vortex) and quantitatively (increased overall secondary flows by about 25%). Much less significant changes were found in the last two stages of the coupling procedure (Figs. 4(b) and (c)). The characteristic spatial structure of the flow field also appears in the temperature contours at this plane (Fig. 5). As expected the second and third level of coupling produce basically identical temperature distributions (hot spot locations and magnitudes) and clearly follow the mean flow trend. Based on the above evidence, in what follows only the results of the third pass calculation are presented and discussed; these are considered to be effectively fully coupled and to be more representative of the flow events in the mixer/nozzle combination.

Streaklines of the predicted velocity field within the lobed mixer are shown in Fig. 6 for axial planes through the lobe peak, midway between peak and trough, and through the lobe trough. In the fan stream the plots suggest a rapid increase of inward radial flows in the region where the main stream flow encounters the fan trough (planes b and c). In the vicinity of the fan trough itself (plane c) the streaklines are nearly aligned with the slope of the lobe contour as would be expected in the absence of flow detachment. Similarly, the core flow in the vicinity of the central plug is parallel to the plug surface. In both cases therefore the ratio of radial to axial velocity near the lobe exit is close to the tangent of lobe and plug penetration angles.

The developing cross-plane flows are seen better in the azimuthal direction plots presented in Fig. 7. At plane d near the inlet to the lobed section the onset of small radial flows can be seen near the inner surfaces of the fan and core sides. In the fan stream they are caused by the recess formed by the hollow annular space separating the two sides while in the core stream they are the result of the angle of the plug. At plane e these inflows have strengthened but are now accompanied by significant swirl velocities on both sides of the lobe contour even though this is still axisymmetric at this plane. This implies a strong upstream influence via the pressure field and is evidently connected to the much stronger circumferential flows that can be seen developing further downstream at planes f and g. The beginnings of a streamwise vortex element centred on the sloping walls of the lobe as early as plane e suggests the strong influence of the downstream flow on the upstream flow development and justifies the retention of the elliptic forms of the equations. It also substantiates the suggestion of Werle *et al.* [1] that the advantage of the lobed mixer against other types of mixers lies in its ability to produce strong axial vorticity at the lobe trailing edge, thus offering the potential for a faster roll up and mixing out of the wake. The orientation and distortion of the streaklines throughout these plots (Fig. 7, planes e–h) suggest momentum transfer from the azimuthal to the radial direction and indicate the strong influence of the lobe geometry on the generation of these pressure driven secondary velocities.

At the mixer exit plane ($x/L_N = 0.3$, plane h) the clockwise rotating vortex (looking downstream) is well established around the lobe surface but the main cross-stream velocities are of radial direction with only small contributions from the azimuthal component near the lobe peak. This suggests that, for the present geometry, the dominant mode of secondary velocity is the turning or flap vorticity as described by Povinelli and Anderson [6]. Radial velocities at this position were 27 and 15% of the inlet axial velocity for the fan and turbine streams, respectively, indicating the substantial strength of the secondary flow. The minor vortices predicted in the trough on the fan side near the turbine side peak, see the regions marked with a circle in Fig. 7 (plane h), are known to exist in this type of mixer. They are considered to arise due to a second mechanism of vorticity generation and are postulated to be of the horseshoe type induced by the interaction of the turbine and fan boundary layers with the leading edges of the lobes. In the present calculations however their direction of rotation is in

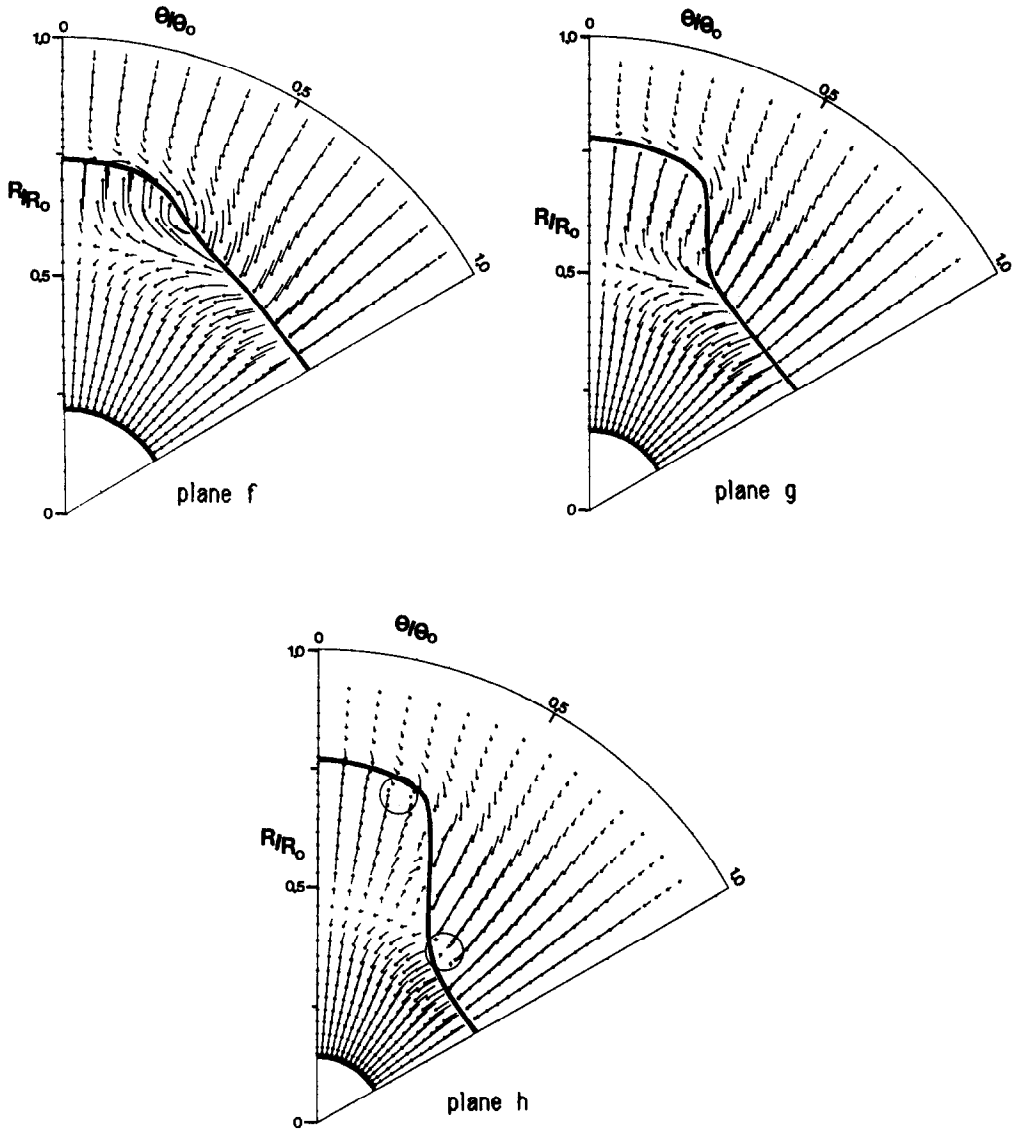

FIG. 7. Predicted flow patterns within lobed mixer: azimuthal planes (looking downstream).

a sense opposite to that expected from a horseshoe vortex type mechanism. The present results would rather suggest that they are the result of separation on the R–θ plane near the exit due to turning of the two streams as the two flows roll around the fan trough and core peak. It should also be noted that these minor vortices were only predicted in the second and third level of coupling. Their strength in the fan and core sides was 7 and 20% of the respective main radial flows at the lobe exit. The flow pattern at the lobe exit does not show any evidence of the passage vorticity mechanism discussed by Povinelli and Anderson [6] and known to be strongest when large lobe penetration and small gaps between the central plug and the lobe trough are used. The geometric features of the present model would seem to exclude this type of mechanism. Inward radial flows near the plug at this position were 30% higher than the outward radial velocities at the core peak.

The predicted secondary flow patterns in the mixing duct are illustrated in Fig. 8 (planes i–k). At $x/L_N = 0.305$ (plane i) the absence of the previously discussed minor vortices supports the claim that they exert negligible influence on the downstream mixing. The region of counter-rotating velocities aligned with the lobe interface can be viewed as a thin vortex sheet emerging from the lobe. At station j located about 20% down the mixing duct the vortex pattern has begun to condense into a more circular shape and by the exit plane its centre of rotation has moved circumferentially towards the centre of the sector. At the nozzle exit plane (Fig. 8, plane k) all velocity magnitudes have decreased and the streakline plot has been repeated using an extended particle tracking time

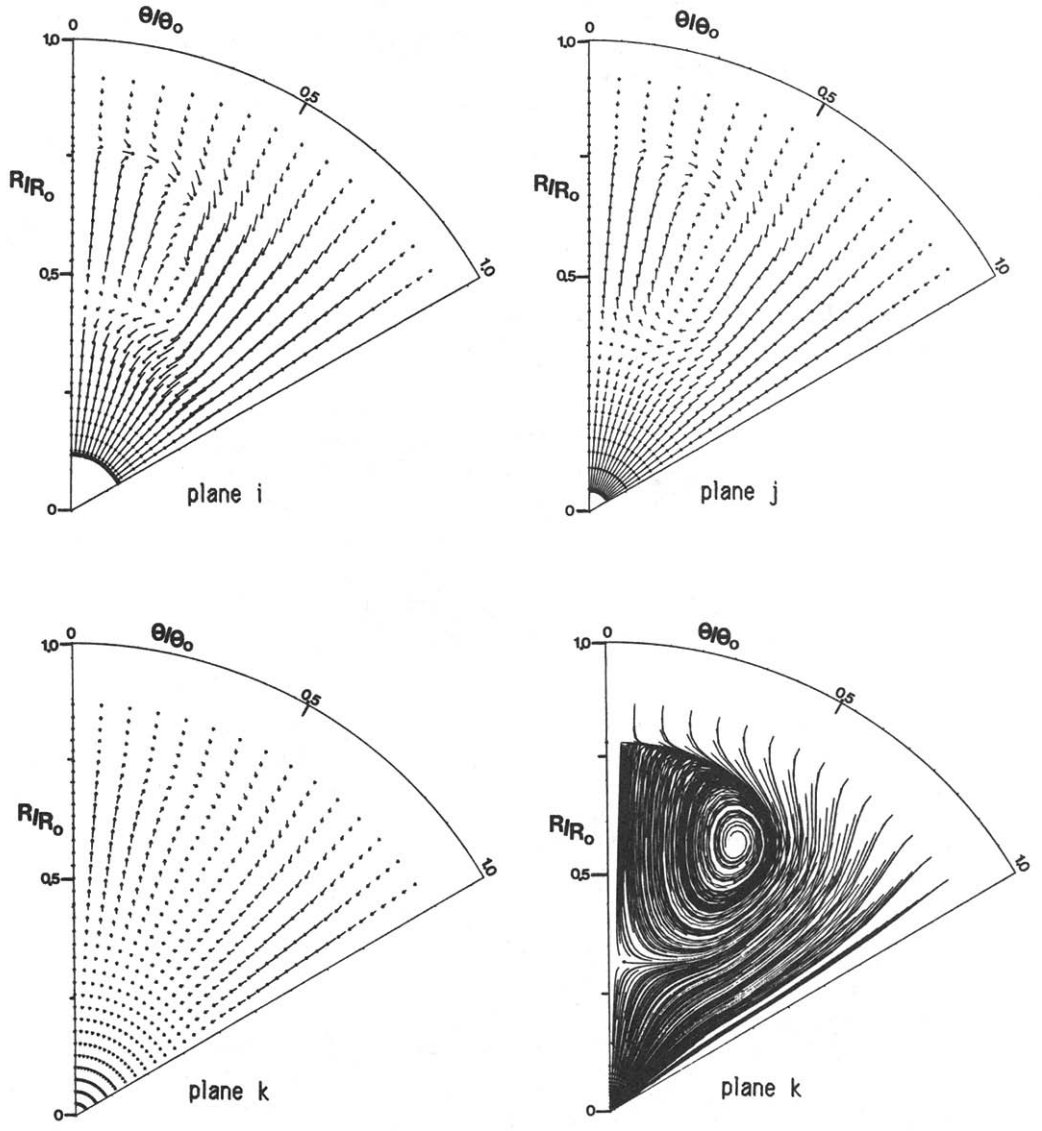

FIG. 8. Predicted flow patterns within mixing duct: azimuthal planes (looking downstream).

to visualize the large vortical structure still persisting at this position. The centre of this vortex is found close to the projected lobe interface. It is clear that the axial vorticity generated within the lobes and emanating from the lobe trailing edge in the form of a vortex cell has been convected throughout the mixing duct length in a stable manner. The strength of this vortex (characterized in terms of maximum radial velocities) was reduced by about 50% over the duct length. The vortex has however grown in scale, so that at the nozzle exit it occupies some 2/3 of the circumference of the sector with inward radial flow filling the rest of the cross-section. The persistence of such a strong vortex system throughout the nozzle has also been found in the investigations of Povinelli and Anderson [6].

It is not surprising that the presence of these secondary motions dominates the heat transfer behaviour in the mixing duct. Figure 9 displays the predicted normalized temperature contours on the axial planes at 0°, 7° and 15°. The penetration of cold fluid (small T^* levels) near the tailpipe wall and hot fluid (large T^*) near the plug, shows the regions of fairly unmixed flow. The closely staggered contours at the top and bottom of the duct (planes a and c) define the thermal mixing layer emerging from the lobe surface. At $\theta = 7°$ (plane b) the wider interface between the two streams corresponds to a larger spread of the mixing layer. The rapid downward movement of the contours on $\theta = 0°$ indicates the incursion of cooler fluid brought from other θ planes by the secondary flow. In contrast the temperature contours on $\theta = 15°$ show a relatively mild behaviour. This is consistent with the secondary flow being purely radial on this plane over the whole mixing duct length; the axial vortex cell has not spread sufficiently to reach $\theta = 15°$ as mentioned

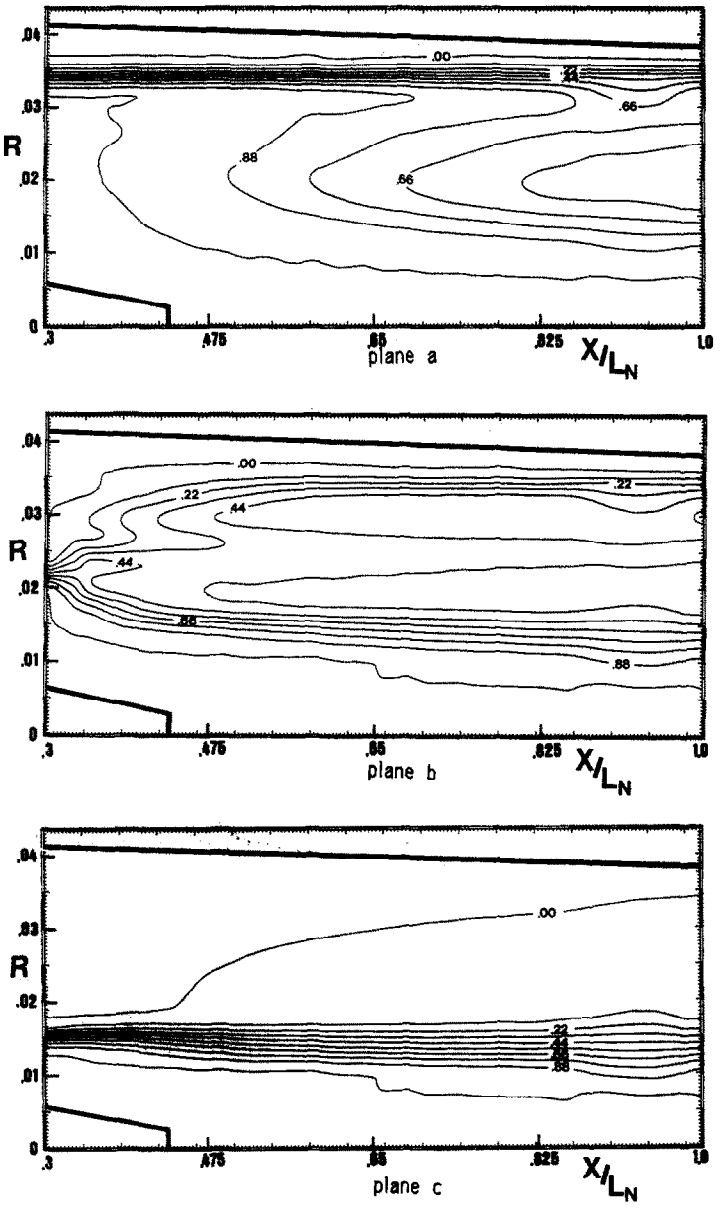

FIG. 9. Predicted temperature contours (T^*) in the mixing duct: axial planes; lobe peak (top), mid-plane (middle), lobe trough (bottom).

above (Fig. 8, plane k). On the intermediate plane the temperature pattern is affected over its whole radial extent. Cross flows in opposite directions at small and large radii mean that cold fluid crosses this plane at small R, but hot fluid is brought in further out, leading to a complex temperature pattern with islands of the same temperature fluid at various radial positions.

The above scenario is supported by the temperature distributions in azimuthal planes depicted in Fig. 10. The temperature gradient region separating the cold and hot streams at plane i (Fig. 10) is roughly aligned with the lobe contour. The increasing spread at plane j and the eventual distortion of the mixing layer at plane k are entirely consistent with the clockwise rotating vortex pattern discussed previously. The sense of mean flow cross plane convection is such as to push cooler fluid in towards the left-hand boundary of the sector and force the hot fluid to split apart, some rising towards the tailpipe wall and some remaining near the engine centre-line. This leads therefore to a bifurcation of the high T^* contours (see for example the 0.66 contours on plane k). By the exit further mixing out of the gradients is evident with an island of hot fluid found isolated roughly in line with the lobe peak projection. The shape of the temperature contours in this region is very similar to that obtained in the computational investigations of Kreskovsky *et al.* [5] and is consistent with the exper-

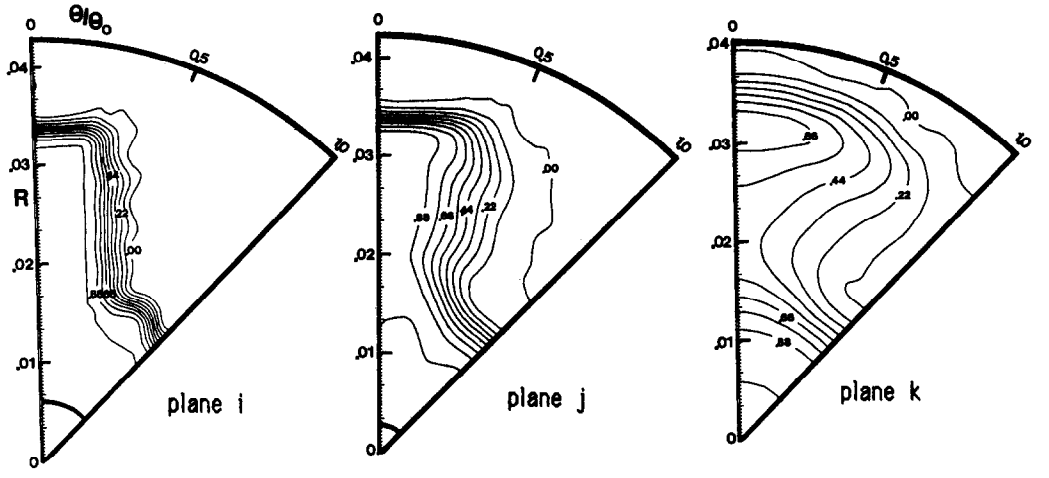

FIG. 10. Predicted temperature contours (T^*) in the mixing duct: azimuthal planes (looking downstream).

imental data of Paterson [9]. Both of the above have used mixers of similar configuration to the present model.

If the increased rate of mixing of the temperature field is the credit size of the forced mixer flow, the increased total pressure losses due to mixing are the debit side. In the present calculations the mass weighted total pressure loss incurred over the lobes themselves corresponds to just over 4% of the inlet dynamic head. Interestingly, the vast majority of this occurred in the bypass stream; this is perhaps not too surprising since the bypass area variation is diffusive whereas the core flow is accelerating. In the mixing duct itself, an additional loss of 1.5% of the dynamic head was predicted with the majority of this taking place in the first 50% of the duct length.

To assess the accuracy of the predicted thermal mixing process, one may turn to the empirical correlation proposed by Frost [17]. He defined the mixing efficiency using the relation

$$\eta = \left(\int T^{0.5}\,\mathrm{d}\dot{m} - T_H^{0.5}\dot{m}_H - T_C^{0.5}\dot{m}_C\right) \Big/ (T_{MIX}^{0.5} \times (\dot{m}_H + \dot{m}_C) - T_H^{0.5}\dot{m}_H - T_C^{0.5}\dot{m}_C)$$

where H and C refer to hot and cold stream and T_{MIX} is the temperature of the completely mixed out stream, i.e.

$$T_{MIX} = (\dot{m}_H T_H + \dot{m}_C T_C)/(\dot{m}_H + \dot{m}_C).$$

Figure 11 shows how this is predicted to vary for the current mixer down the length of the mixing duct. The empirical function deduced from several experimental surveys by Frost correlates η against a geometric parameter depending on mixer perimeter, mixing duct length and mixing duct diameter. For the present system Frost's correlation (deduced from several mixers including ones of similar configuration to that used here) gives a value of η of 62% at the tailpipe exit whereas the predictions in Fig. 11 show a value of 58%. It seems then that at least the overall thermal mixing efficiency of the current predictions is in good agreement with available experimental knowledge.

SUMMARY

A finite volume procedure capable of calculating the flow and heat transfer within complex three-dimensional geometries has been used to compute the aerodynamic flow and associated temperature mixing within a turbofan lobed mixer nozzle. The calculation started upstream of the lobes and the lobe flow prediction provided the necessary inlet boundary conditions for the downstream mixing duct calculation. In the present analysis the dependence of previous methods on measurements to provide these necessary secondary flows at the lobe exit has been removed. A clear illustration is given of the necessity to include an interaction region at the end of the mixer lobes for satisfactory predictions.

The results demonstrated the ability of the present method to predict the streamwise vorticity generated within the lobes. It is these large-scale vortex patterns which are known to be the dominant mechanism con-

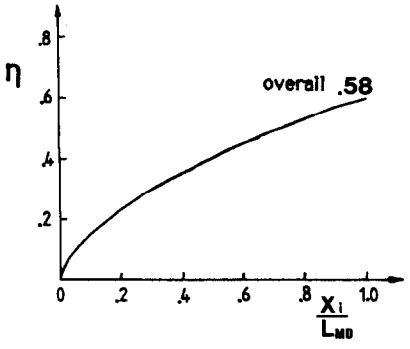

FIG. 11. Predicted mixing efficiency in mixing duct.

trolling and enhancing mixing in the downstream region. The plausibility of the predicted mean velocity fields in the mixer/nozzle combination was demonstrated using streakline visualization of the flow. For the temperature field, the development of isolated hot spots was shown to be consistent with the predicted vortex pattern, and was similar to that observed in previous experimental studies. The potential usefulness of the method to designers was underlined by presenting predicted values for such important parameters as total pressure loss and mixing efficiency. These calculations go a long way towards boosting confidence in the applicability of the method to the study of forced mixer systems. It remains to be confirmed whether the accuracy is sufficiently high to enable the small but significant improvements sought by designers to be successfully predicted. A more detailed testing of the predictions against experimental measurements is the next crucial step. Such work is planned for the near future before proceeding to use the method to evaluate the effectiveness of various mixer designs (e.g. geometrical changes, bypass ratio changes, inlet swirl effects, etc.).

Acknowledgements—The work reported here has been supported by Rolls-Royce plc. The authors would like to acknowledge their gratitude for this support and the many useful discussions with staff of the Powerplant Technology section at Rolls-Royce (Derby).

REFERENCES

1. M. J. Werle, R. W. Paterson and W. M. Presz, Flow structure in a periodic axial vortex array, AIAA Paper 87-0610 (1987).
2. S. F. Birch, G. C. Paynter, D. B. Spalding and D. G. Tatchell, Numerical modelling of three dimensional flows in turbofan engine exhaust nozzles, *J. Aircraft* **15**, 489 (1978).
3. J. M. Barton and S. F. Birch, Numerical modelling of three dimensional turbulent jet flows, AIAA Paper 80-0008 (1980).
4. S. V. Patankar and D. B. Spalding, A calculation procedure for heat, mass and momentum transfer in three-dimensional parabolic flows, *Int. J. Heat Mass Transfer* **15**, 1787 (1972).
5. J. P. Kreskovsky, W. R. Briley and H. McDonald, Investigation of mixing in a turbofan exhaust duct. Part I: analysis and computational procedure, *AIAA J.* **22**(3), 374 (1984).
6. L. A. Povinelli and B. H. Anderson, Investigation of mixing in a turbofan exhaust duct. Part II: computer code application and verification, *AIAA J.* **22**(4), 518 (1984).
7. W. R. Briley and H. McDonald, Analysis and computation of viscous subsonic primary and secondary flows, AIAA Paper 79-1453 (1979).
8. B. H. Anderson and L. A. Povinelli, Factors which influence the behaviour of turbofan forced mixer nozzles, NASA TM-81668 (1981).
9. R. W. Paterson, Turbofan mixer nozzle flow field—a benchmark experimental study, *ASME J. Engng Gas Turbines Pwr* **106**, 692 (1984).
10. T. J. Barber, G. L. Muller, S. M. Ramsey and E. M. Murman, Three dimensional inviscid flow in mixers. Part I: mixer analysis using a Cartesian grid, *AIAA J. Propul. Pwr* **2**(3), 275 (1986).
11. T. J. Barber, G. L. Muller, S. M. Ramsey and E. M. Murman, Three dimensional inviscid flow in mixers. Part II: analysis of turbofan forced mixers, *AIAA J. Propul. Pwr* **2**(4), 339 (1986).
12. P. Koutmos, J. J. McGuirk, C. H. Priddin and M. N. Sodha, Numerical investigation of the flow within a turbofan lobed mixer, Report FS/88/9, Mech. Engng Dept, Imperial College, London (1988).
13. W. P. Jones and B. E. Launder, The prediction of laminarisation with a two equation model of turbulence, *Int. J. Heat Mass Transfer* **15**, 301 (1972).
14. B. E. Launder and D. B. Spalding, The numerical computation of turbulent flow, *Comput. Meth. Appl. Mech. Engng* **3**, 269 (1974).
15. S. V. Patankar, *Numerical Heat Transfer and Fluid Flow*. Hemisphere, Washington, DC (1981).
16. P. Koutmos, An isothermal study of gas turbine combustor flows, Ph.D. Thesis, University of London (1985).
17. T. H. Frost, Practical bypass mixing systems for fan jet aero engines, *Aeronaut. Q.* 141 (May 1966).

MODIFICATION DES CHAMPS DE VITESSE ET DE TEMPERATURE A L'ENTREE D'UN MELANGEUR A HELICE

Résumé—On décrit une procédure de calcul des champs de vitesse et de température dans une combinaison tuyère/mélangeur à hélice. Les résultats ont été obtenus à partir d'une procédure de volume finis pour des équations elliptiques tridimensionnelles. Les écoulements sont déterminés dans des géométries complexes à partir d'un système de mailles non alignées de façon que l'écoulement puisse être prédit dans les lobes mêmes. La turbulence est représentée par le modèle à deux équations k–ε. La performance du mélangeur est dominée par un arrangement périodique de cellules tourbillonnaires axiales créé par la géométrie du lobe. On examine la dépendance des méthodes de calcul antérieurs pour les conduits de mélange vis-à-vis des vitesses secondaires mesurées dans le plan de sortie du lobe. La présente étude montre sa capacité à prédire le développement aval des mouvements secondaires à grande échelle et leur grande influence sur la signature en température à la sortie de la tuyère. On présente aussi la capacité de la méthode à prédire les paramètres principaux aux concepteurs des mélangeurs, tels que la pression totale et l'efficacité. Les résultats obtenus illustrent la potentialité de la méthode pour fournir une technique flexible d'analyse du système complet tuyère/mélangeur.

MODELLIERUNG DES ERZWUNGENEN STRÖMUNGS- UND TEMPERATURFELDES IN EINER VENTILATOR-MISCHDÜSE

Zusammenfassung—Es wird ein Rechenverfahren vorgestellt, mit dem das Strömungs- und Temperaturfeld in der Mischdüse eines mehrblättrigen Ventilators berechnet werden kann. Die stationären dreidimensionalen elliptischen Gleichungen werden mit Hilfe eines Finite-Volumina-Verfahrens gelöst. Mit dem vorgestellten Rechenverfahren kann das Strömungsfeld durch Verwenden eines uneinheitlichen Gitternetzes innerhalb komplizierter Geometrien berechnet werden, sodaß auch Strömungsberechnungen zwischen den Vertilator-Flügeln möglich sind. Die Turbulenz wird mit Hilfe des k–ε Modells beschrieben. Es zeigt sich, daß Mischungserscheinungen infolge einer Reihe periodisch auftretender, axialer Wirbelkeime, die durch die Flügelgeometrie entstehen, überwiegen. Die zur Strömungsberechnung im Bereich des Mischkanals notwendigen Randbedingungen am Flügelaustritt erhält man durch Berechnung der großen Sekundärgeschwindigkeit, die von der Verwirbelung innerhalb und am Austritt der Flügel abhängt. Damit ist es möglich, die seither verwendeten Rechenverfahren für Mischungskanäle unabhängig vom Vorhandensein gemessener Sekundärgeschwindigkeiten im Austrittsgebiet der Flügel anzuwenden. Es wird die Leistungsfähigkeit des vorgestellten Verfahrens gezeigt, bei der Vorhersage der stromabwärts gerichteten Entwicklung von Sekundärbewegungen und ihrem großen Einfluß auf das Temperaturprofil am Düsenaustritt. Anhand von Beispielen wird gezeigt, daß die zur Beurteilung von Mischern wichtigen Parameter wie absoluter Druckverlust und Mischungswirkungsgrad mit Hilfe des Rechenverfahrens ermittelt werden können. Die Folgerichtigkeit der erhaltenen Ergebnisse weisen das vorgestellte Verfahren als geeignet aus, komplette Mischdüsen-Systeme flexibel beurteilen zu können.

МОДЕЛИРОВАНИЕ ПОЛЕЙ ТЕМПЕРАТУРЫ И СКОРОСТИ В ТУРБОВЕНТИЛЯТОРЕ С СОЧЕТАНИЕМ СМЕСИТЕЛЕЙ И СОПЕЛ

Аннотация—Описана методика расчета полей скорости и температуры в многолопастном турбовентиляторе с сочетанием смесителей и сопел. Решения получены методом конечных объемов для стационарных трехмерных эллиптических уравнений течения жидкости. Методика позволяет рассчитывать течения для сложных геометрий с использованием системы криволинейных сеток непосредственно внутри лопастей. Турбулентность моделируется на основе двухпараметрической k–ε модели турбулентной вязкости. Показано, что на характеристики вынужденного течения в смесителе влияет периодическая решетка осевых вихревых ячеек, образованная лопастями. Расчет больших вторичных скоростей, связанных с завихренностью внутри и на выходе из лопастей, дает необходимые граничные условия на выходе для определения течения в канале смешения. Это устраняет зависимость предыдущих расчетных методов для каналов смешения от измеренных вторичных скоростей в выходной плоскости лопасти. Показано, как с помощью данного метода можно определять развитие крупномасштабных вторичных движений вниз по течению, а также их сильное влияние на температуру у выхода из сопла. Представлены также результаты, иллюстрирующие возможности метода при расчете важных параметров смесителей: общей потери давления и эффективности смесителя. Достоверность полученных результатов позволяет применить метод для анализа всей системы смесителей и сопел.